Numerical Model for Saturated-Unsaturated Flow in Deformable Porous Media 3. Applications

T. N. NARASIMHAN AND P. A. WITHERSPOON

Earth Sciences Division, Lawrence Berkeley Laboratory and Department of Materials Sciences and Mineral Engineering University of California, Berkeley, California 94720

This is the third and conclusive part of a three-paper series and describes the application of a numerical model for saturated-unsaturated flow in deformable porous media. In all, 10 illustrative examples are presented not only to demonstrate the validity of the method but also to highlight the fundamental unity that exists in the basic principles of the fields of hydrogeology, soil mechanics, and soil physics. The chosen examples involve such diverse phenomena as soil consolidation, infiltration, and drainage and generation of fluid pressures due to cyclic loading such as earthquakes.

INTRODUCTION

A theory and a numerical algorithm were presented in parts 1 and 2, respectively, of this series of papers for numerical analysis of fluid flow in saturated-unsaturated deformable porous media [*Narasimhan and Witherspoon*, 1977; *Narasimhan et al.*, 1978]. In this concluding part we present examples illustrating the validity of the model and its applicability to a variety of problems related to the flow of water in subsurface systems. The examples have been chosen from the fields of soil mechanics, soil physics, and hydrogeology and have been selected partly to illustrate the power of the numerical model and partly to demonstrate the conceptual unity that underlies these fields. The sample problems relate to purely saturated flow with soil deformation, purely unsaturated flow, saturated-unsaturated flow, and, finally, the generation of pore pressure in soil masses due to earthquake vibrations. The examples are listed below.

1. Under saturated flow with consolidation we will consider consolidation in a heterogeneous doubly draining clay column, simulation of field consolidation observed at Pixley, California, due to periodic water level changes, and consolidation of a column of clay slurry.
2. Under unsaturated flow we will consider infiltration into a moderately saturated soil, infiltration into a column of extremely dry soil, and axisymmetric flow to a soil-water sampler.
3. Under saturated-unsaturated flow we will consider drainage from a one-dimensional soil column, drainage from a sandbox, and consolidation around an excavation in soft clay.
4. Under pore pressure generation and dissipation we will consider pore pressure generation and dissipation in a three-dimensional system.

All the aforesaid examples were solved by using the computer program Trust described in part 2 [*Narasimhan et al.*, 1978].

SATURATED FLOW WITH CONSOLIDATION

Consolidation in a Heterogeneous Doubly Draining Clay Column

The problem of land settlement associated with clayey soils is of considerable interest in the field of soil mechanics. To study such problems, the one-dimensional consolidation theory of *Terzaghi* [1925] has been used to great practical advantage by many soil engineers on the assumption that horizontal strains are negligible and that all the deformation takes place in the vertical direction. Although the Terzaghi theory provided reasonable results in many field cases, it is known that in many other field situations the theory predicted smaller settlements or consolidation than was actually observed. While there may be several plausible explanations for the discrepancy between theory and field observations, *Schiffman and Gibson* [1964] reasoned that the variation of permeability with depth in clayey materials may be an important factor. To verify their hypothesis, they considered a doubly draining 30.48-m column of London blue clay (Figure 1) with depth-dependent permeability and compressibility coefficients (Figure 2). Treating K and m_v as continuous functions of depth and using a finite difference scheme, Schiffman and Gibson computed compaction as a function of time. The same problem was also solved by our numerical model, the column being divided into 10 different materials with a stepwise variation of material properties (Figure 2) and 100 volume elements being used. A comparison of our numerical results and those of *Schiffman and Gibson* [1964] is presented in Figure 3. As is shown in Figure 3, the agreement between the two results is reasonable, and the small differences observed are probably to be attributed to the different techniques employed for handling the spatial variation of material properties. In addition to computing the gross consolidation of the clay column the solution procedure also yielded data on the propagation of the strain wave within the column (Figure 4). As one would expect, at early times the regions close to the top and the bottom of the doubly draining system experience maximum deformation rates. With time, however, the strain field gradually migrates inward toward the interior portions of the system, as is seen in Figure 4.

Simulation of Field Consolidation Observed at Pixley, California

The subsidence of land surface in many young alluvial basins due to the withdrawal of groundwater and the consequent decline in pore pressures is widely known [*Poland and Davis*, 1969]. An extremely well documented field example of this occurs near Pixley in the San Joaquin Valley of California. The subsidence of land surface and the associated piezometric levels near Pixley have been measured carefully over several years by the U.S. Geological Survey [*Lofgren and Klausing*, 1969] and are presented in Figure 5. Recently, *Helm* [1975] successfully modeled observed compaction at Pixley over a 12-year

Paper number 8W0689.

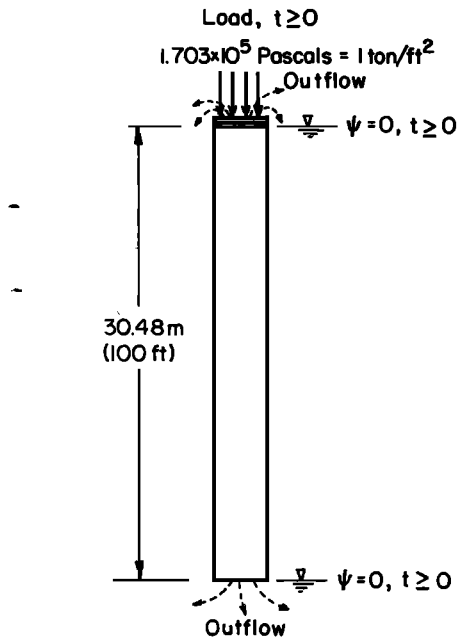

Fig. 1. Compaction of a heterogeneous clay column: initial and boundary conditions.

period from 1958, treating the observed piezometric fluctuations as the mechanism causing subsidence.

Within the alluvial sediments at Pixley there exist 21 compacting beds of various thicknesses, aggregating a total of 85 m and separated by hydraulically continuous highly permeable sand beds. In his mathematical simulation of Pixley subsidence, *Helm* [1975] assumed that practically all the observed consolidation could be accounted for in the clay beds and that consolidation in the sand beds was negligible. Furthermore, he found that for purposes of mathematical simulation the actual system can be treated as equivalent to 17 uniform beds, each 4.877 m thick and having $K' = 2.9 \times 10^{-11}$ cm/s, $S_{s,\text{virgin}} = 7.54 \times 10^{-4}$ m^{-1}, and $S_{s,\text{elastic}} = 1.51 \times 10^{-4}$ m^{-1}. Here, $S_{s,\text{virgin}}$ denotes the specific storage coefficient under normal loading conditions, while $S_{s,\text{elastic}}$ denotes the same coefficient under conditions of rebound or recompression.

To validate our numerical model with an example from the field, the Pixley consolidation was simulated as a one-dimensional consolidation problem, modeling one of the 17 doubly draining clay layers. On symmetry considerations, only one half of the clay column need be modeled.

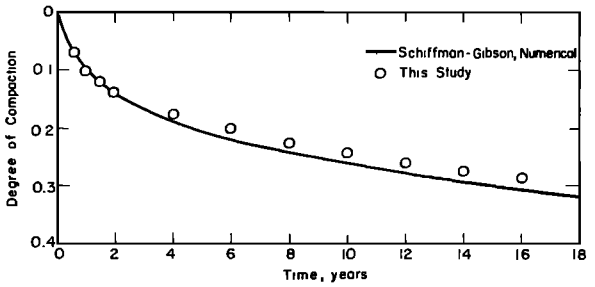

Fig. 3. Compaction of a heterogeneous clay column: a comparison of numerical results.

The column was discretized into 20 elements, each 0.122 m thick and subjected to a time-dependent boundary condition consisting of hydrographs of day by day variations in the piezometric heads in the aquifer. The initial distribution of pore pressure was assumed to be hydrostatic, while that preconsolidation stress was assumed to vary parabolically from the bottom to the center of the bed, as was done by *Helm* [1975]. The initial and boundary conditions used are shown in Figure 6. A period of 4000 days from October 21, 1958, was simulated. A comparison of the numerical results obtained during the present study with the observed field data is presented in Figure 7, which shows reasonable agreement between the two, with a maximum deviation of about 7% in early 1964. A similar accuracy was also obtained by *Helm* [1975]. For the period 1966–1968, Helm obtained slightly better agreement than this study. In this regard, it may be pointed out that Helm plotted the cumulated compaction of 21 beds of varying thicknesses, while Figure 7 relates to 17 beds of the same thickness.

Consolidation of a Column of Clay Slurry

An extreme case of the soil consolidation phenomenon is that of shrinkage of an active clay such as bentonite. Such materials can undergo very large changes in volume over relatively short intervals of time. The movement of water in such swelling soils may sometimes be of interest, e.g., self-weight filtration [*Smiles*, 1974]. An important task here is to establish

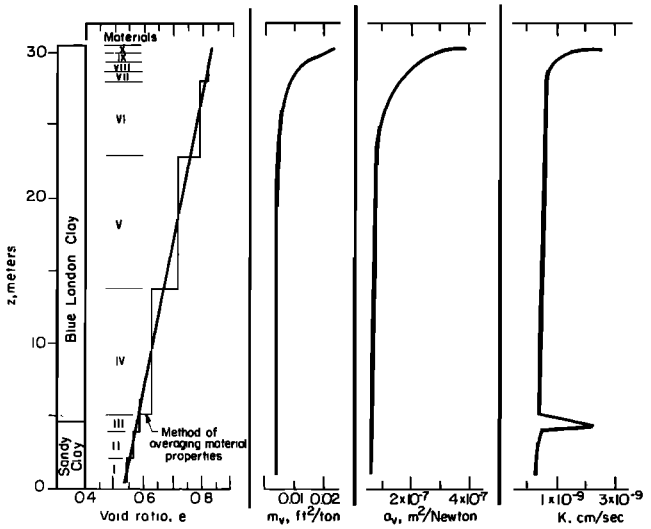

Fig. 2. Compaction of a heterogeneous clay column: depth-dependent material properties.

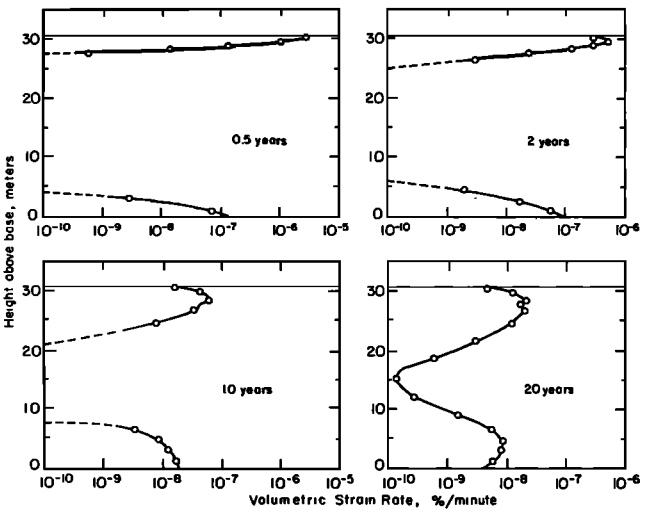

Fig. 4. Compaction of a heterogeneous clay column: the volumetric strain rate as a function of depth.

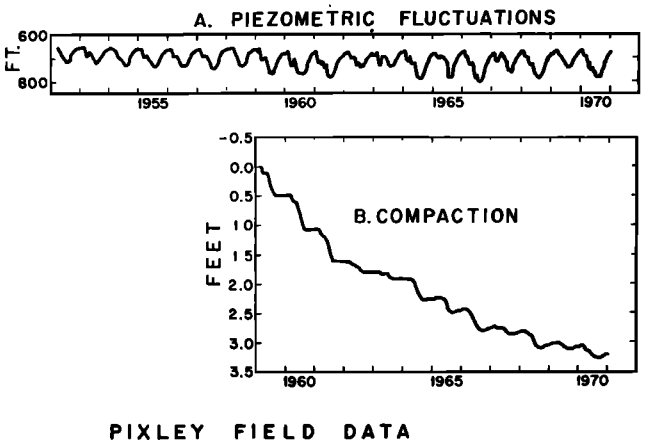

Fig. 5. Land subsidence at Pixley, California: observed piezometric fluctuations and land subsidence [after *Helm*, 1975].

the hydraulic conductivity of such materials as a function of void ratio.

Smiles and Rosenthal [1968] developed a theory for the one-dimensional movement of water in clay-water systems that are free to swell in the direction of water movement. This theory was developed from the fact that Darcy's law describes fluid flow with reference to the movement of soil particles, and is based on a scale of length defined with reference to the distribution of the mass of clay. In the new material scale the diffusion equation is an appropriate expression with which to describe fluid movement.

Smiles and Rosenthal considered the desorption (drainage) of electrolyte from a semiinfinite column of saturated clay that is restrained within smooth cylindrical walls but is free to contract in the direction of the cylindrical axis. For this system they defined a new material scale

$$m = \int_0^x \frac{dx}{1+e} \tag{1}$$

In this scale the continuity equation for an elemental volume dV can be shown to be

$$\frac{\partial}{\partial m}\left(D_m \frac{\partial e}{\partial m}\right) = \frac{\partial e}{\partial t} \tag{2}$$

in which

$$D_m = \frac{K}{1+e}\frac{\partial x}{\partial e} \tag{3}$$

The semiinfinite colume is subject to the following initial and boundary conditions:

$$\begin{aligned} e &= e_n \qquad m > 0 \qquad t = 0 \\ e &= e_0 \qquad m = 0 \qquad t > 0 \end{aligned} \tag{4}$$

If Boltzmann's transformation $\lambda = mt^{-1/2}$ is used, as suggested by *Bruce and Klute* [1956], the quantity D_m can be experimentally determined by

$$D_m(e) = -\frac{1}{2}\frac{d\lambda}{de}\int_{e_n}^{e} \lambda \, de \tag{5}$$

If it is valid, this theory must lead to the following consequences.

1. The moisture content, or equivalently the void ratio, must be uniquely related to λ.

2. The cumulative outflow from the column, or equivalently the change of length of the column, must plot as a straight line with the square root of time.

3. The slope of the straight line in consequence 2 should be numerically equal to the integral

$$\frac{dL}{dt^{1/2}} = \int_{e_n}^{e} \lambda \, de \tag{6}$$

In order to verify their theory, Smiles and Rosenthal conducted a set of experiments with a 13.5-cm-tall Perspex column filled with a slurry of Wyoming bentonite at an initial void ratio of $e_n = 44.76$ (with a porosity of 97.81%). A constant air pressure of 1.66 m of water was applied at the top, while at the bottom, $m = 0$, water was allowed to drain freely through a millipore filter, as is shown schematically in Figure 8. The void ratio e_0 ($m = 0$, $t > 0$) was maintained at 15.91 (94.08%). The nonlinear relationship between e and effective stress for Wyoming bentonite was independently determined experimentally, and this relation is plotted in the form of a semilog plot in Figure 9*a*. The slope of the straight line in Figure 9*a* is the compression index C_c, for Wyoming bentonite.

The desorption experiments were carried out for 3 weeks, during which the shrinkage of the column at various times and the void ratios within the column at various times were measured. Graphs of shrinkage versus time$^{1/2}$ and e versus λ were plotted. As was predicted by the theory, shrinkage versus time$^{1/2}$ was indeed found to plot as a straight line with a slope of $dL/dt^{1/2} = 3.8 \times 10^{-3}$ cm/s$^{1/2}$. Also according to theory there was a fairly well defined relation between $\lambda = mt^{-1/2}$ and void ratio, and on graphical evaluation the integral

$$\int_{e_n}^{e_0} \lambda \, de$$

yielded a value of 3.2×10^{-3} cm/s$^{1/2}$. The difference between this value and the value of 3.8×10^{-3} cm/s$^{1/2}$ (see (6)) was attributable to experimental errors.

Using the λ versus e relation and (5), Smiles and Rosenthal proceeded to compute $D_m(e)$. The value of $D_m(e)$, so computed, considered in conjunction with the e versus effective stress relation shown in Figure 9*a*, directly leads to the evaluation of hydraulic conductivity K of the Wyoming bentonite as a function of void ratio (Figure 9*b*).

The numerical model developed by us was applied to the Smiles-Rosenthal problem for the reverse purpose of predicting shrinkage, the known moisture characteristic relation of Figure 9*a* and the K versus e relation deduced from Smiles-Rosenthal experiments being assumed.

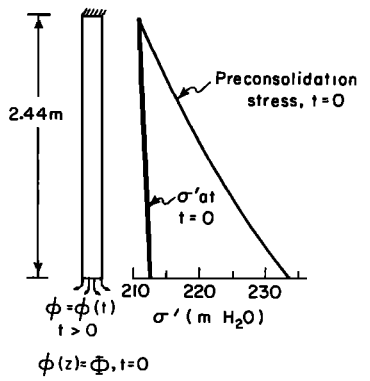

Fig. 6. Land subsidence at Pixley, California: initial and boundary conditions.

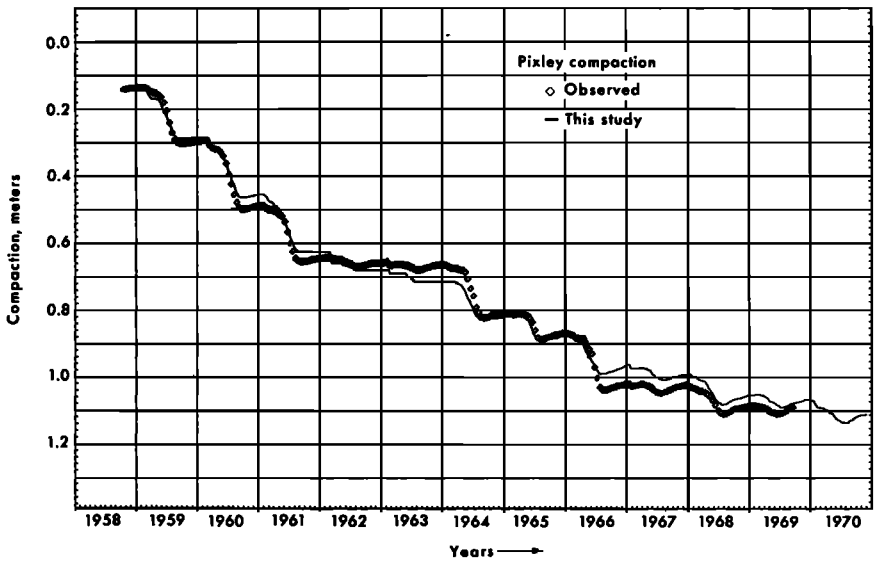

Fig. 7. Land subsidence at Pixley, California: a comparison of observed and numerical results.

It should be pointed out here that the Boltzmann transformation is strictly applicable to a horizontal column. For convenience, however, the experiment had to be conducted with the column in a vertical position. Nevertheless, the potential gradient component due to gravity was less than 8% and hence could be neglected.

The numerical simulation was carried out to investigate (1) whether the shrinkage computed with the numerical model agreed reasonably with the actual observations, (2) whether the role of gravity was important, and (3) the extent to which attention needed to be given to a material coordinate system in studying the highly compressible system under consideration.

Lagrangian formulation. Under saturated flow conditions the discretized equations for an element n may be written as

$$\sum_m K_{m,n} \frac{(z_m - z_n) + (\psi_m - \psi_n)}{(d_{n,m} + d_{m,n})} \Gamma_{m,n} = (M_c)_n \frac{\Delta \psi_n}{\Delta t} \qquad (7)$$

Note that (7) is actually related to a material element fixed in the soil particles [*Narasimhan and Witherspoon,* 1977]. In other words each element is defined as having a constant volume of solids.

Since the bulk volume of the element n changes with time, it follows that the geometrical quantities $\Gamma_{m,n}$, the surface area between the elements m and n; $d_{m,n} + d_{n,m}$, the distance between the nodal points m and n; and z_m, z_n, the elevations of nodal points, should all change with time. In evaluating the left-hand side of (7) therefore these time-dependent changes must be given due consideration. For slightly deforming systems it is customary to ignore these time-dependent changes.

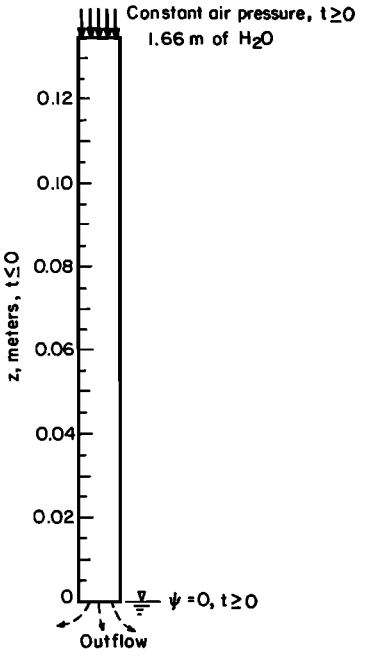

Fig. 8. Consolidation of clay slurry: initial and boundary conditions.

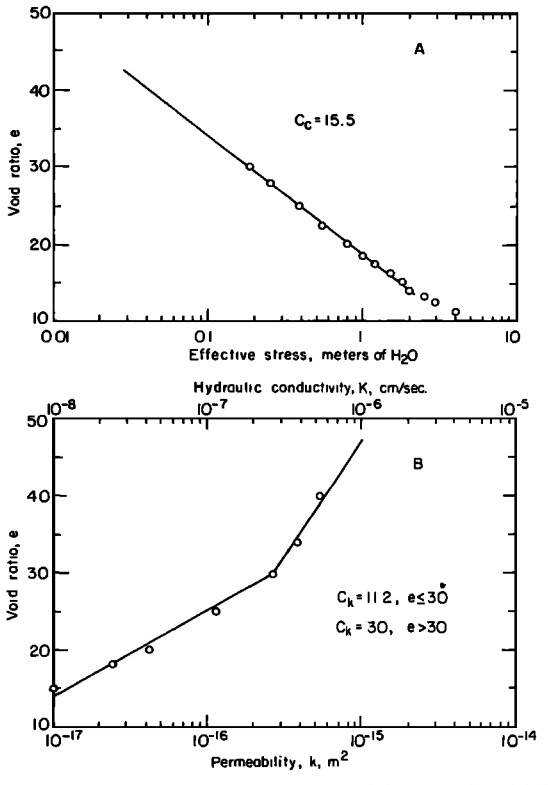

Fig. 9. Consolidation of clay slurry: material properties. (a) Void ratio versus effective stress. (b) Void ratio versus permeability.

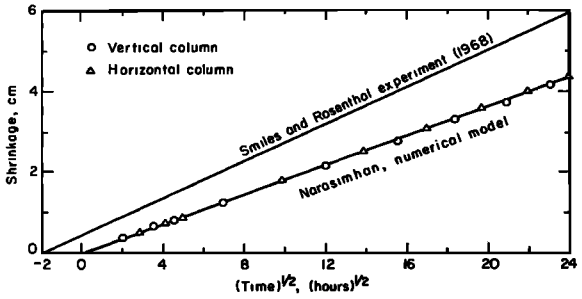

Fig. 10. Consolidation of clay slurry: a comparison of numerical and experimental results.

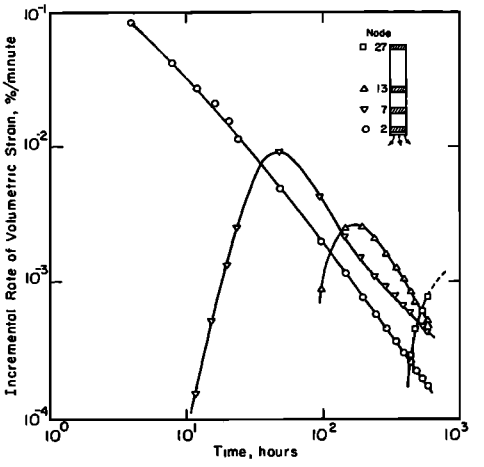

Fig. 11. Consolidation of clay slurry: volumetric strain rates of some typical elements.

However, can they be ignored without loss of accuracy in the case of a highly consolidating column of clay slurry? To investigate this, we pose the problem in Lagrangian coordinates, as described below.

Note that because the problem under consideration is one-dimensional, the surface areas $\Gamma_{m,n}$ in (7) are invariant with time. In order to take into account the temporal variations of the z and d in (7) the coordinates of nodal points were recalculated at the end of each time step in the light of past deformation history. In addition, the time rates of change of z and d were also estimated at the end of each time step. By using these data the mean values of $\bar{z}_m$, $\bar{z}_n$, $\bar{d}_{m,n}$, and $\bar{d}_{n,m}$ were computed in the same manner as that in which other nonlinear coefficients were estimated [*Narasimhan et al.*, 1978]. These mean values were then used to solve (7).

Horizontal versus vertical column. The first phase of the study consisted in simulating consolidation, with (1) the column being vertical and (2) the column being horizontal. The boundary and initial conditions are shown in Figure 8. In the vertical column the initial void ratio e_n was uniformly 44.43 (with a porosity of 97.74%), while at $m = 0$, for all t, e_0 was equal to 15.54 (with a porosity of 93.58%). The condition of uniform void ratio, and hence uniform effective stress, caused a decrease in hydraulic potential from 1.779 m of H_2O at the bottom to 1.774 m at the top. As a result, at $t = 0$ there was a small vertical movement of water toward the top. In the horizontal column the initial void ratio was uniformly 44.76 (with a porosity of 97.81%), while the constant value ratio e_0 at $m = 0$ was 15.05 (with a porosity of 93.78%).

The computed values of consolidation for the horizontal and vertical columns are presented in Figure 10. It is readily seen from the figure that both horizontal and vertical columns agree very well in predicting total consolidation. However, detailed examination of the computed results showed that the pattern of consolidation of similarly located volume elements within the two columns was considerably different. For example, in the vertical column the upward movement of water persisted for over 10 days, during which the volume elements in the upper part underwent swelling. On the other hand, none of the elements in the horizontal column experienced any swelling.

The pattern of deformation occurring within the column is illustrated in Figure 11. It is seen that for each element the strain rate initially increases with time, attains a peak, and finally declines with time. Moreover, nodes located away from the draining end attain peak strain rates at progressively later times, showing the migration of the consolidation transient.

Departure from experimental results. In referring back to Figure 10 it is immediately seen that the numerical results show smaller consolidation than the experimental observations. To investigate this discrepancy, the numerical results were first checked for internal consistency. In this regard we see from Figure 10 that the shrinkage versus $t^{1/2}$ plot is indeed a straight line, passing through the origin, which is in accordance with theory. Also, for the vertical column a plot of λ versus e is shown in Figure 12. According to theory, this plot reveals a fairly well defined unique dependence of e on λ. Furthermore, the theory predicts that the slope of the shrinkage versus $t^{1/2}$ line in Figure 10 should be equal to the integral

$$\int_{e_n}^{e_0} \lambda \, de.$$

Graphical evaluation of this integral from Figure 12 was found to be 3.1×10^{-3} cm/s$^{1/2}$, while the slope of the straight line in Figure 10 worked out to be 3.06×10^{-3} cm/s$^{1/2}$.

The consistency of the numerical model having been examined, it was reasonable to question whether the discrepancy was because the input values of permeability were smaller than they ought to be. Trial computations showed that good agreement could be obtained between the numerical and the observed results if the input data on permeability were multiplied by an arbitrary factor of 2.

A reexamination of the data (D. E. Smiles, personal communication, 1974) suggested that the experimental results were subject to errors due to difficulties involving measuring shrinkage and computing void ratios. On considering the experimental difficulties the discrepancy between numerical and experimental results appears reasonable.

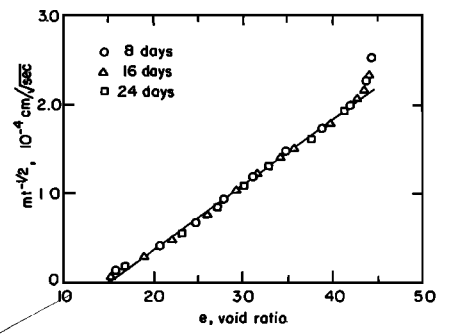

Fig. 12. Consolidation of clay slurry: the relation between λ and e for the vertical column.

Accuracy and adjustments of nodal distances. Note that the Lagrangian treatment requires periodic adjustments of the geometric parameters, nodal distances, elevations, surface areas, and volumes. Computationally, while it is fairly easy to make adjustments to nodal volumes occurring in the term M_c on the right-hand side of (7), it is far more cumbersome to make such adjustments to nodal elevations, distances, and surface areas.

Since volume involves third power of distances, the geometric parameter likely to undergo maximum change is nodal volume. Also, it is seen from the left-hand side of (7) that nodal surface areas occur in the numerator and nodal distances in the denominator, which suggests that the changes in these quantities would tend to compensate for each other. It seems reasonable to infer that except in extreme cases, neglecting to adjust nodal distances, elevations, and surface areas on the left-hand side of (7) may not adversely affect accuracy.

In the one-dimensional problem under study it is recognized that, $\Gamma_{n,m}$ being constant, nodal volume change is of the same order of magnitude as change in nodal distance or elevation. This problem therefore poses an extreme case in which errors due to neglecting changes in nodal distances are likely to be maximum, and hence the problem merits further attention.

Figures 13*a* and 13*b* show the plots of shrinkage versus time$^{1/2}$ computed with a mesh in which the quantities z_m, z_n, and $d_{m,n}$ were held constant on the left-hand side of (7) while the variation of nodal volume (incorporated in the M_c term on the right-hand side) was allowed to vary in accordance with deformation. For convenience we will call this a 'rigid' mesh. Now, since the column is consolidating, the nodal points must move toward each other with time, and hence the nodal distances must continuously decrease with time. Since this decrease in nodal distances is ignored in the rigid mesh, the gradients are underestimated, and the fluxes calculated on the left-hand side of (7) tend to be smaller than they would otherwise be. As a consequence, the rigid mesh solution yields a much slower consolidation history than the rigorous solution in Figure 13*a*.

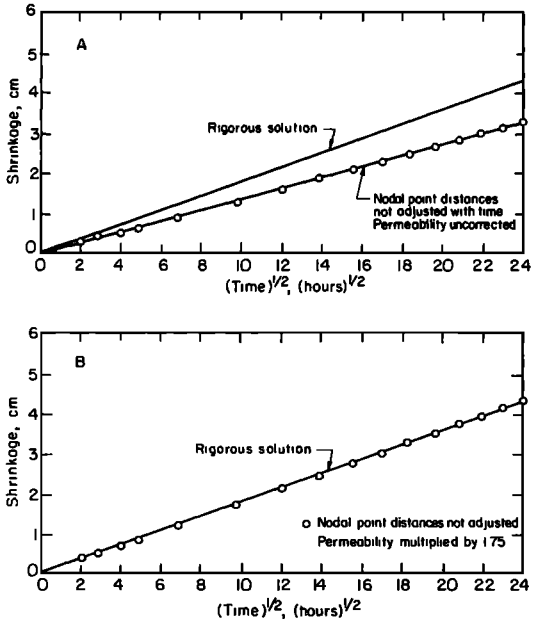

Fig. 13. Consolidation of clay slurry: the effect of ignoring nodal point displacements on the rate of consolidation. (a) Permeability uncorrected. (b) Permeability multiplied by 1.75.

TABLE 1. D Versus θ Relation for the Absorption Problem

θ	D, cm^2/s
0.2376	0
0.2440	1.59×10^{-4}
0.2569	2.13×10^{-4}
0.2698	2.82×10^{-4}
0.2826	3.29×10^{-4}
0.2955	3.73×10^{-4}
0.3084	4.51×10^{-4}
0.3213	6.31×10^{-4}
0.3341	7.91×10^{-4}
0.3470	7.96×10^{-4}
0.3599	7.20×10^{-4}
0.3727	6.69×10^{-4}
0.3856	6.66×10^{-4}
0.3985	6.80×10^{-4}
0.4113	7.43×10^{-4}
0.4242	8.55×10^{-4}
0.4371	9.99×10^{-4}
0.4500	1.31×10^{-3}
0.4628	1.98×10^{-3}
0.4757	3.34×10^{-3}
0.4886	1.04×10^{-2}

In looking at the left-hand side of (7) it can be reasoned that instead of continuously adjusting to the d and z, one could, from a purely computational point, keep the mesh rigid and apply an equivalent correction to the permeability term $K_{m,n}$. With this reasoning in mind the permeability values in the rigid mesh problem were uniformly multiplied by 1.75 (by shifting the e versus log k plot appropriately to the right in Figure 9*b*), and the calculations repeated. The results are presented in Figure 13*b*. It is readily seen that the rigid mesh solution with adjusted permeability does indeed agree with the rigorous solution. These results lead to some inferences of practical interest.

1. A single simple correction to permeability seems capable of adequately compensating for the far more complex task of deforming the mesh with time.

2. In the particular problem studied, the equivalent correction turned out to be multiplication by a factor of 1.75 (increasing permeability by 75%). However, the precision of measuring the permeability function experimentally is such that an error of 100% may often be tolerable. Thus the error accrued owing to the use of the rigid mesh appears to be of the same order of magnitude as that introduced owing to errors in the input values of permeability.

3. In the present problem the total shrinkage at the end of 24 days was 32% of the original column length. During this period the maximum strain attained by the bottommost element was 64%. Despite the large deformations involved, the required permeability correction was only 75%. In actual field problems, far smaller deformations are likely to be encountered, and the required permeability corrections are likely to be so small that they should be well within the precision of experimentally measuring permeability.

4. For most field problems therefore one could use a rigid mesh without any permeability corrections and still obtain reasonably accurate results. Nevertheless, if one still desired to minimize errors, one could use appropriate permeability corrections. A possible method for determining the correction factors would be to carry out parametric studies. The correction factors determined from such parametric studies could be expressed in terms of C_c or total deformation.

Deforming and nondeforming coordinates. In discussing the concept of specific storage, *De Wiest* [1969] drew attention to

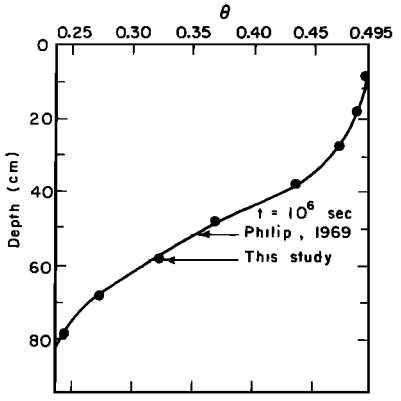

Fig. 14. Infiltration into a moderately saturated soil: a comparison of results.

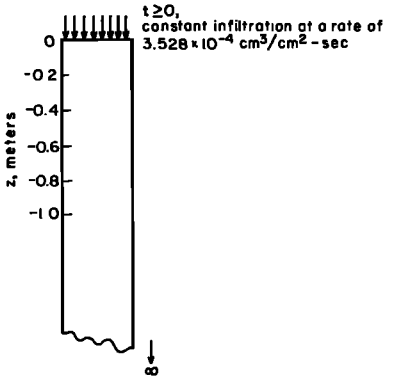

Fig. 15. Rain infiltration: initial and boundary conditions.

the fact that *Jacob*'s [1950] derivation of the governing equation of groundwater flow considers a deformable volume element for the time derivative part, while on the spatial derivative part it considers a nondeformable element. To get over this inconsistency, De Wiest then proceeded to redefine specific storage in a fixed coordinate system.

If we consider a saturated flow region and neglect water compressibility, it is obvious that the volume of the flow region must decrease by an amount equal to the volume of water released from storage. Therefore it is not physically realistic to assume that the overall dimensions of the flow region do not change with time. The formulation based on a deforming volume element is therefore more logical. In the light of our study of the results from a rigid mesh we can interpret Jacob's derivation as pertaining to a deforming volume element but ignoring, as a reasonable approximation, the effects of deformation on surface areas and nodal distances in evaluating fluxes. Viewed in this fashion, Jacob's derivation is of practical utility.

UNSATURATED FLOW

Infiltration Into a Moderately Saturated Soil

The next example deals with the early absorption stage of infiltration into a vertical unsaturated soil column. Initially, the soil is at a uniform moisture content of $\theta = 0.238$. At time $t = 0$ the top of the column is brought to a state of saturation at $\theta_{sat} = 0.495$, and this boundary condition is maintained indefinitely. If one is interested only in the early absorption history or if the soil column is horizontal, then gravity is unimportant. Then the governing equation can be written in the form of the diffusivity equation

$$\frac{\partial}{\partial z}\left(D(\theta)\frac{\partial \theta}{\partial t}\right) = \frac{\partial \theta}{\partial t} \tag{8}$$

in which z is the depth below the soil surface and $D(\theta)$ is the diffusivity coefficient. For the particular soil considered, D is a highly nonlinear function of θ as given in Table 1.

This problem was solved by using the numerical technique of this study, by discretizing the flow region into 45 volume elements, each 2 cm long. The resulting moisture content profile at $t = 10^6$ is presented in Figure 14 and is compared with the analytical solution of *Philip* [1969]. The agreement is obvious.

In connection with the solution of this problem it must be pointed out that an arithmetic mean was used to evaluate the interface permeabilities (or diffusivities) rather than the harmonic mean permeability. The reason for this is explained in the next section, dealing with an extremely dry soil column.

Infiltration Into a Column of Extremely Dry Soil

The problem of infiltration into extremely dry soils is of considerable interest in the field of agriculture. In considering soil-water relations during rain infiltration, *Rubin and Steinhardt* [1963] showed that ponding of water on the soil surface can occur only if rainfall intensity exceeds the saturated soil permeability. If it does not, the soil will tend to attain that uniform saturation at which rainfall intensity exactly matches hydraulic conductivity. To demonstrate this, they considered a vertical semiinfinite column of Rehovot sand (with a porosity of 39.7%) on whose surface rain was assumed to fall at a constant rate (Figure 15). The sand itself was initially very dry (with a saturation of 12.6% and a moisture content of 0.05%). The hydraulic conductivity K and moisture content θ of Rehovot sand are highly nonlinear functions of moisture content (Figure 16). Empirically, these functions were fitted to the following equations by *Rubin et al.* [1964]:

$$-\psi = 11.3 + (3.19/\theta) - 0.05e^{15} + e^{-575\theta} + 16.3 \tag{9}$$

in which ψ is in millibars, and

$$K = 8400/(-\psi^5 + 14.45^5) \tag{10}$$

in which K is in centimeters per second. Because of the extremely dry nature of the soil the initial pressure head within the column was very low and was computed from (8) to be -6.69×10^3 m of water. Computations based on (9) and (10)

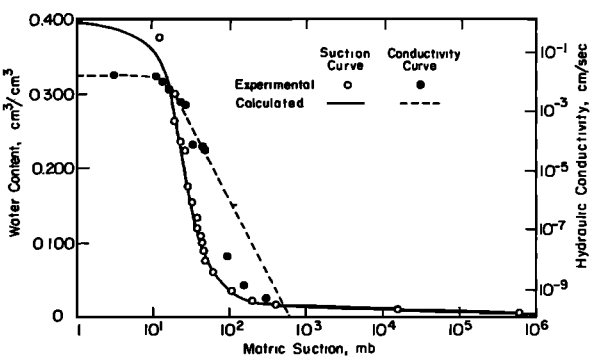

Fig. 16. Rain infiltration: material properties [after *Rubin et al.*, 1964].

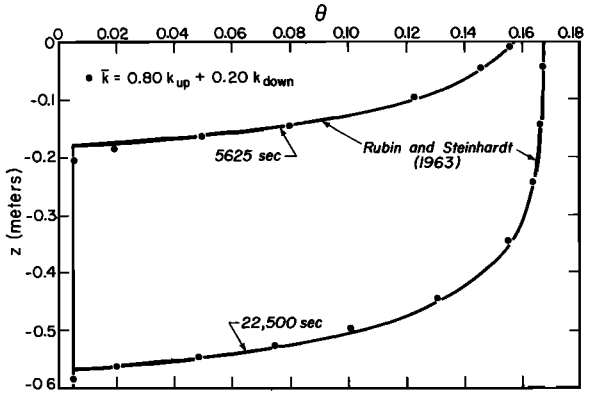

Fig. 17. Rain infiltration: a comparison of numerical results.

showed that at a moisture content of ≈0.168 and a pressure head of ≈−0.3 m of water the hydraulic conductivity of the soil will equal the assumed rainfall intensity of 3.528×10^{-4} cm/s.

Rubin and Steinhardt [1963] posed the infiltration problem outlined above in the form of the diffusivity equation and solved it with the help of a finite difference scheme. Their results are shown by the solid lines in Figure 17.

Although the diffusivity formulation is useful in solving the aforementioned highly nonlinear problem, it has been rightly pointed out [*Bruce and Klute*, 1956] that the diffusivity equation cannot be used when the porous medium is heterogeneous. This is because of the jump discontinuity of the θ distribution at the material interface. It is therefore desirable to be able to solve the infiltration problem with ψ as the dependent variable. However, owing to the strong nonlinearity of the coefficients relative to ψ, the solution of the ψ-dependent equation is considered difficult. For example, *Neuman* [1972], who attempted to solve the above problem using the Galerkin finite element method, found that the infiltration process could not even be initiated with the ψ-dependent formulation and concluded that the diffusivity formulation was the best way to solve the problem.

Recent application of the Trust computer program has shown that it is indeed possible to solve the infiltration problem by using the ψ-dependent governing equation. The key to the understanding of the problem here is that of determining the appropriate mean permeability at the interface between two volume elements. Recall from equation (3*a*) of part 2 of this series of papers [*Narasimhan et al.*, 1978] that in the

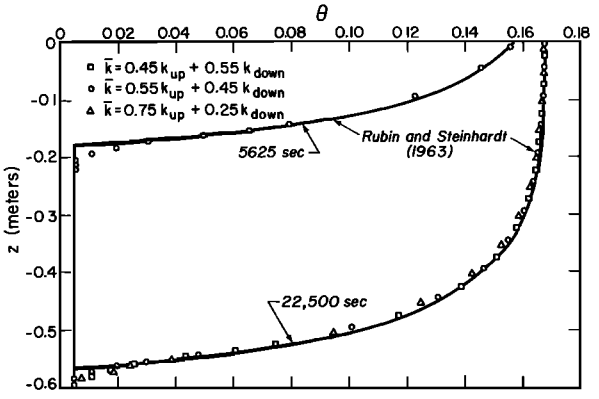

Fig. 18. Rain infiltration: the effect of permeability weighting on the numerical solution.

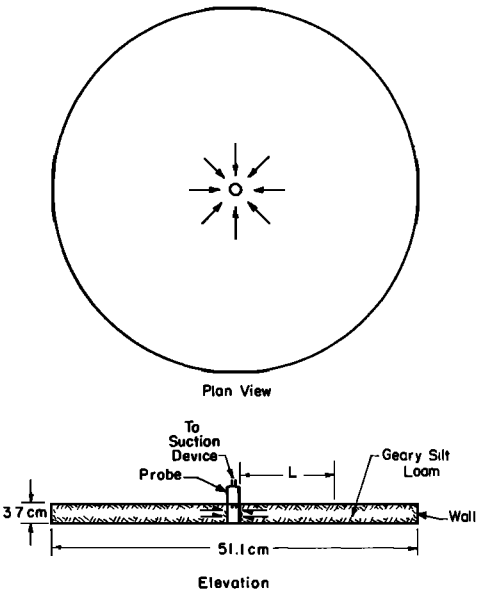

Fig. 19. Radial flow to a soil probe: a physical description of the model.

present work the mean interface permeability has been defined as being the harmonic mean permeability

$$\bar{K}_{l,m} = \frac{K_l K_m (d_{l,m} + d_{m,l})}{K_m d_{l,m} + K d_{m,l}} \tag{11}$$

This mean assures continuity of fluxes at the interface and is found to be a good estimate in linear and moderately nonlinear problems. However, owing to the occurrence of the product $K_l K_m$ in the numerator of (11), $\bar{K}_{l,m}$ tends to be strongly weighted toward the lower of the two permeabilities. As a result, in extremely dry soils, permeability of the interface just ahead of the front becomes too low to drain the fluid effectively on the downstream side. This in turn causes abnormal buildup of potential in the volume element. It therefore appears that a mean value based on a higher weight for the upstream permeability is necessary for handling this problem.

Accordingly, it was first decided to use an arbitrary definition of $\bar{K}_{l,m}$ according to

$$\bar{K}_{l,m} = 0.8 K_{\text{upstream}} + 0.2 K_{\text{downstream}} \tag{12}$$

Moreover, two further precautions are needed before attempting to solve the problem. First, because of the abruptness of the boundary condition at $t = 0$, to start the problem smoothly, it is necessary to keep the time steps relatively small during the initial stages of calculations. Second, because the present algorithm uses a quasi-linearization technique in which a mean value of permeability over a time step is estimated and used in the calculations, it becomes necessary to limit the time steps to small magnitudes so that the permeability and capacity coefficients do not vary widely from one time step to the next.

The flow region was discretized into volume elements 0.01 m wide. The dependence of S on ψ and K on ψ was approximated by means of tables with over 90 data points with linear interpolation. The size of Δt was gradually increased from 0.1 s to a maximum of 8 s. Since the stable time step was never below 10 s, it was possible to carry out the calculations explicitly. The results obtained are shown compared with Rubin and Steinhardt's results in Figure 17. It is seen that the agreement

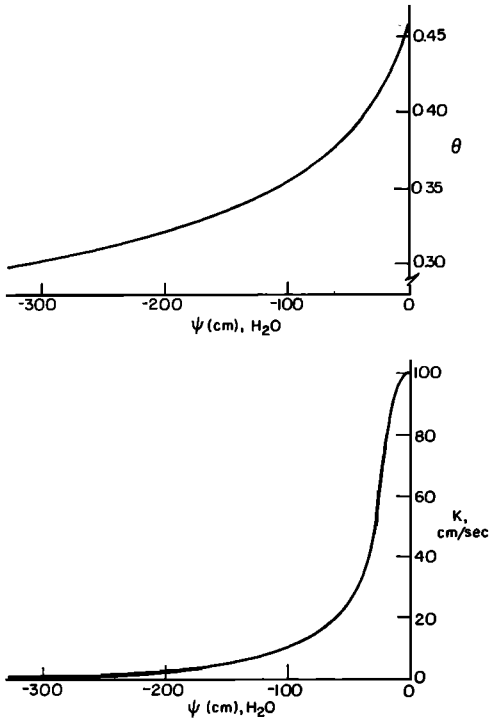

Fig. 20. Radial flow to a soil probe: physical properties of Geary silt loam.

is generally good. A check on the mass balance showed mass balance errors to be less than 0.1% at the end of 22,500 s.

As is seen in (12), a factor of 0.8 is used for upstream weighting. This choice is arbitrary, and the arbitrariness does indeed call into question the credibility of the solution process. To study this question further, different weighting schemes were studied for $t > 5625$ s. The results are presented in Figure 18. It is surprising to note from Figure 18 that the solution is to a large extent insensitive to the choice of the weighting function, and indeed one does not incur any significant error if one simply chooses arbitrarily to use the arithmetic mean. However, it must be mentioned here that in the early stages of the solution process it is indeed necessary to use a high upstream weight of 0.8.

An attempt was made to solve this problem implicitly by increasing Δt to 20 s. This gave poor results due to large variations in permeability and specific moisture capacity from one time to another.

Axisymmetric Flow to a Soil-Water Sampler

A practical problem of the soil scientist is to obtain a sample of soil solution from a small region surrounding the sampling device. In order to justify confidence in the sampling procedure it is essential to understand in detail the flow field around the sample, especially when the solution is rapidly moving past the probe. For this purpose the present numerical model was used to simulate radial flow to a soil probe in partially saturated soils.

The physical model (Figure 19) consists of a horizontal layer of wet Geary silt loam in an impermeable cylindrical shell with a porous probe at its center. It is assumed that the model is suitably protected from evaporative losses. It is also assumed that through an elaborate experimental setup the effluent can be continuously withdrawn for volume measurement while a constant suction at the probe can be simultaneously applied.

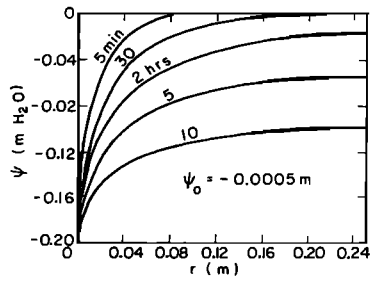

Fig. 21. Radial flow to a soil probe: spatial distribution of ψ at different times.

The model is subjected to several cycles of different suction, as follows. The soil is first saturated with water and brought to a constant suction and moisture content by applying a controlled probe suction until all outflow has ceased. An additional known suction is then applied, and the outflow rate observed. Similar routines are repeated at other suctions, and the results compared.

In the numerical problem the probe was assumed to be 3.7 cm tall, 1.1 cm in diameter in a cylindrical sample, and 51.1 cm in diameter. The physical properties of the silt loam (Figure 20) were obtained from *Hanks and Bowers* [1962]. The flow region was discretized into 30 cylindrical volume elements, the innermost 10 being 0.5 cm wide and the rest 1 cm wide. The soil was assumed to be rigid and nonswelling. Because of the small height of the sample, gravitational effects were neglected.

Numerical solutions were generated for various simulated sampling routines to evaluate the spatial distribution of pressure head and moisture content as well as the rate of flow into the soil probe. A few of the results are summarized below.

Figure 21 shows the spatial variation of pressure head ψ produced by a suction of 0.2 m at the probe, corresponding to an initial soil suction of -0.0005 m. For the same conditions, Figure 22 shows the spatial distribution of soil moisture content θ, and Figure 23 depicts cumulative outflow at the probe as a function of time.

The quantity of solution released from storage by different parts of the flow region to make up the effluent withdrawn at the probe is illustrated in Figure 24. It is seen that at early times a bulk of the cumulative drainage takes place in the immediate vicinity of the probe. As time progresses, more of the depletion from storage occurs in the regions away from the probe. It may be pointed out here that owing to the cylindrical symmetry of the flow region, the outer shells have far greater volumes than the inner ones, and hence, despite the relatively small changes in moisture content, the outer shells can dominate the contribution to total cumulative depletion from storage.

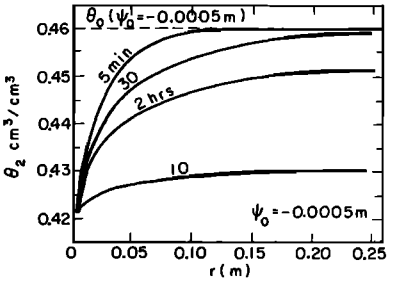

Fig. 22. Radial flow to a soil probe: spatial distribution of θ at different times.

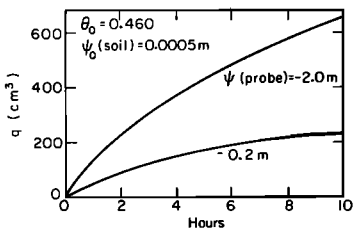

Fig. 23. Radial flow to a soil probe: cumulative volume of the effluent as a function of time.

SATURATED-UNSATURATED FLOW

Drainage From a One-Dimensional Soil Column

Liakopoulos [1965] conducted several experiments on the drainage of water from vertical columns of Del Monte sand. One of these experiments was chosen for simulation by the present model.

A 1-m-high Perspex column (Figure 25) was packed with Del Monte sand and was instrumented with a sufficient number of tensiometers to measure continuously moisture tension at various points within the column. Prior to the start of the experiment ($t < 0$), water was continuously added from the top of the column and allowed to drain freely at the bottom through a micropore filter. The flow was carefully regulated until all tensiometers read zero pore pressure. This meant that the vertical gradient in potential equals unity ($\partial\phi/\partial z = 1$). On obtaining this initial condition the addition of water from the top was discontinued, and the upper boundary rendered impermeable. From then on ($t > 0$) the tensiometer readings were recorded while the flow rates at the draining end were being periodically measured.

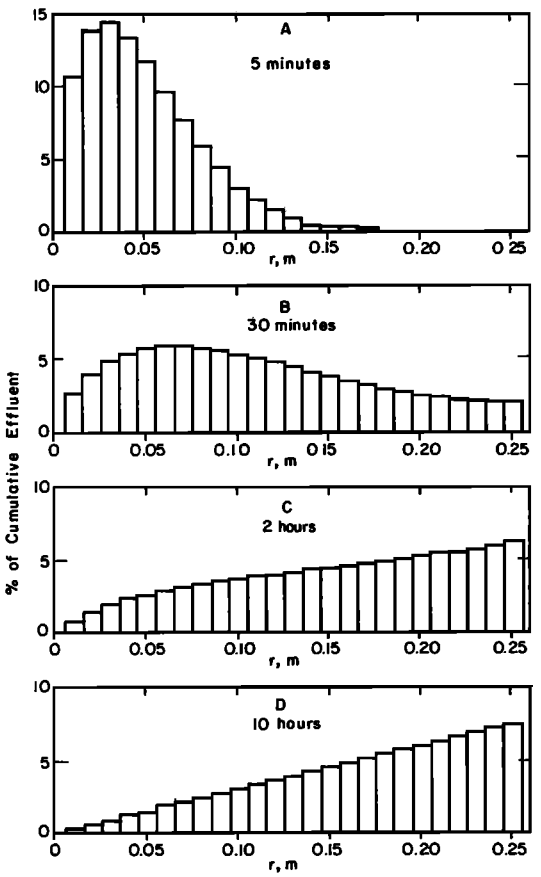

Fig. 24. Radial flow to a soil probe: the percentage of contribution to cumulative depletion from storage by 1-cm-wide shells of the flow region.

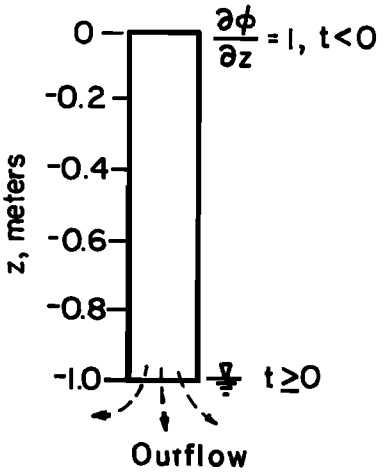

Fig. 25. One-dimensional column drainage: initial and boundary conditions.

The physical properties of Del Monte sand were measured by Liakopoulos by an independent set of experiments. The sand had a porosity of 29.75%. The dependencies of θ, S, and k as deduced from the experimental data [*Liakopoulos*, 1965] are given in Figure 26. It can be seen from the figure that both θ and S remain unchanged in the range -0.2 m $\leq \psi \leq 0$. In other words, moisture suction has to exceed the 'air entry' value of -0.2 m before the pores can be desaturated; that is, the soil remains saturated because ψ remains negative but greater than -0.2 m.

For purposes of numerical simulation the column was divided into 10 volume elements of equal size. As a first step in the simulation, the sand was assumed to be nondeformable and rigid, as is customarily done in dealing with unsaturated flow. The profiles of pore pressure distribution, computed in this fashion, are shown in Figure 27*a*. It is seen that although the computed values agree reasonably with the experimentally observed values after about 10 min of starting the experiment, the computed suctions are markedly greater than the observed suctions at the end of 5 min. Note from the figures that at the end of 5 min the observed pressure is everywhere greater than -0.2 m. In light of the saturation and moisture content curves of Figure 26 this means that no drainage could have occurred during the first 5 min, since the soil is rigid and the expansivity of water is extremely small. Yet experimental observations (Figure 28) indicate that the drainage had indeed occurred during the first 5 min. The most reasonable conclusion that one can draw from this is that during the first 5 min the drained water was released from storage by a slight deformation of the soil skeleton and a consequent decrease in void volume.

The next question to be considered then is whether better simulation of experimental results could be achieved by assuming the sand to be deformable.

To assess the importance of deformation, the sand was assigned a C_c value of 0.017, which was assumed to be reasonable for an unconsolidated sand. At $t = 0$ the effective stress at a point 0.55 m from the top was computed to be 0.825 m of water or 8.1 N/m². At this effective stress a C_c of 0.017 amounts to an a_v of approximately 2.1×10^{-6} m²/N ($m_v \approx 1.7 \times 10^{-6}$ m²/N).

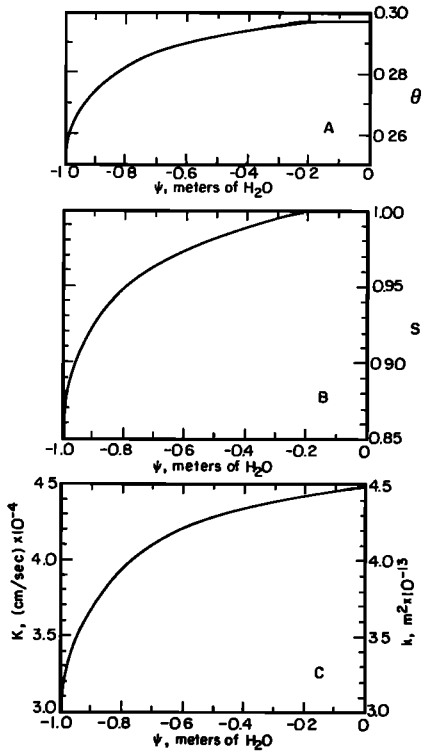

Fig. 26. One-dimensional column drainage: material properties.

Using the assumed value, we carried out a second simulation, assuming that all the moisture suction developed was fully converted to effective stress according to the relation $\sigma' = \sigma - \rho_w g \psi$. This is equivalent to setting $\chi = 1$ in (13) of part 1 [*Narasimhan and Witherspoon*, 1977]. The results of this simulation are given in Figure 27*b*. It can now be seen that there is a closer agreement between the results at the end of 5 min, but for longer times the computed pore pressures are consistently larger than the observed pressures, a finding that suggests that the fluid mass capacities of the volume elements are larger than they should be. Such indeed will be the case if the elements are deforming in addition to desaturating.

From Figures 27*a* and 27*b*, one could infer that while deformation is important at small values of suction (and hence small values of time), it must drastically decrease, or even cease to exist, at higher magnitudes of suction. If this were so, χ could not be unconditionally set to 1 in the unsaturated zone but should be a function of ψ. In the absence of any data on the χ versus ψ relationship for Del Monte sand the following arbitrary assumption was made,

$$\begin{aligned} \chi &= 1 \qquad \psi \geq -0.2 \text{ m} \\ \chi &= 0 \qquad \psi \leq -0.2 \text{ m} \end{aligned} \tag{13}$$

implying that the flow is purely saturated when ψ is greater than air entry value and purely unsaturated otherwise.

The results obtained on the basis of (13) in conjunction with $C_c = 0.017$ are given in Figure 27*c*. It can now be seen that there is reasonable agreement between experimental and observed results at early as well as late times.

The results presented in Figure 28 show a good agreement between the experimental and computed drainage rates. The simulations described above strongly suggest that in certain types of problems the importance of deformation cannot be ignored when the soil is under moisture suction.

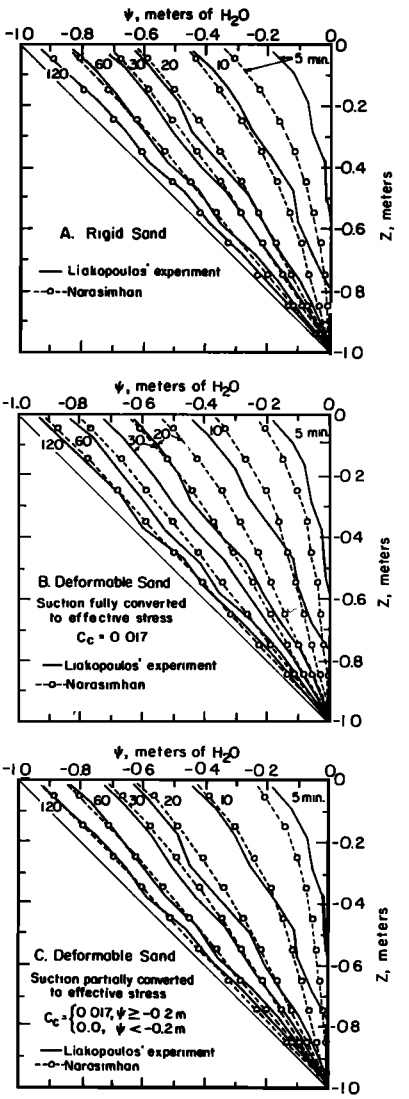

Fig. 27. One-dimensional column drainage: a comparison of numerical and observed pressure head profiles.

Drainage From a Sandbox

The next problem concerns the simulation of saturated-unsaturated flow in a two-dimensional sandbox. *Vachaud et al.* [1971] conducted very carefully controlled drainage and infiltration experiments on a sandbox 3 m long, 2 m high, and 0.05 m thick. The particular experiment chosen for numerical simulation is schematically described in Figure 29. In this experiment the sandbox was first allowed to attain hydrostatic equilibrium with the water levels on the left- and right-hand sides of the sandbox standing at an elevation of 1.43 m above the

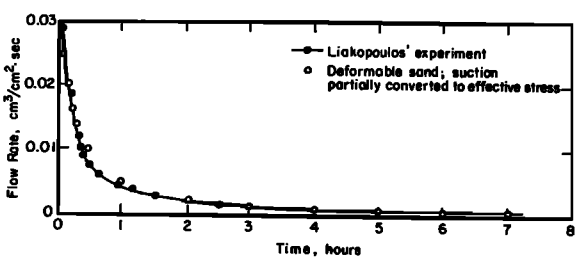

Fig. 28. One-dimensional column drainage: a comparison of numerical and experimental drainage rates.

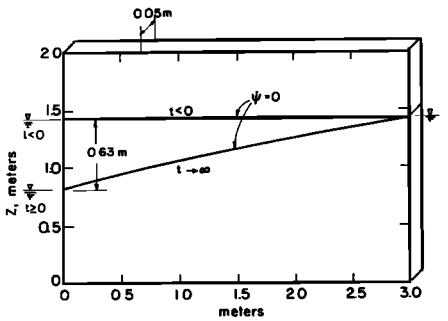

Fig. 29. Drainage from a sandbox: initial and boundary conditions.

base for a long period of time. Then at $t = 0$ the water level on the left-hand side was allowed to drop by 0.63 m to 0.8 m above the base and was maintained at that elevation for the duration of the experiment. During this experiment, lasting for over 50 hours, pressure heads were monitored in 20 tensiometers distributed over the sandbox, and the distribution of moisture content was also periodically monitored. These data enabled the determination of the distribution of ϕ, ψ, and θ over the sandbox and the change in the quantity of stored water in the system.

The aims of the simulation were to use the known material properties and boundary conditions and to determine the temporal and spatial variations of ψ and θ and the change in the stored water.

The experimentally determined relationships between ψ and θ and hydraulic conductivity are shown in Figure 30. It can be seen from the figure that the experimental data points show considerable scatter. But for purposes of simulation the sand was assumed to be homogeneous with mean properties corresponding to the solid lines shown in the figure. The mean values used are shown in Figure 31.

According to the authors of the experiment there was hydrostatic equilibrium at $t = 0$. Accordingly, for purposes of simulation, hydrostatic initial conditions were used, as is shown in Figure 32.

In the simulations, three different values of deformation parameters were considered: $C_c = 1 \times 10^{-6}$ (for rigid sand), $C_c = 5 \times 10^{-4}$, and $C_c = 1 \times 10^{-2}$ (for the most deformable case). In addition, χ was set to 1 for $\psi \geq -0.2$ and to zero otherwise. Comparison of the results showed that since the problem is dominated by the phenomenon of desaturation, there was practically no difference in the results obtained with the three different values of soil deformation.

As a first step in the comparison of experimental and numerical results, the computed position of the surface $\psi = 0$ is compared with the experimental data in Figure 33. As can be seen, but for slight departures at early times, the agreement is reasonable, considering the difficulties associated with the experiment.

A special feature of the experiment was the measurement of the spatial and time-dependent variations of moisture content at different points in the sandbox. Thanks to this, the experiment also yielded data on the quantity of water removed from storage in the sandbox. A comparison of the numerical and experimentally observed cumulative depletion from storage is shown in Figure 34. It is seen from this figure that although the two curves approach each other toward steady state ($t > 50$ hours), they depart significantly between 1 and 20 hours during the transient behavior. This suggests that the mean physical properties used in the simulation are not quite appropriate.

A detailed comparison of the experimentally observed isopotential lines with the computed ones [*Narasimhan*, 1975] showed that these agreed very well over most of the flow region except at the upper left-hand portion. A careful study of the computed results showed that over 55% of the total depletion from storage occurred in a part of the unsaturated zone about 1 m long and 0.7 m high, located in the upper left-hand part of the sandbox. Moreover, this region was also experiencing maximum moisture suctions and hence the lowest permeabilities within the flow region.

It was brought to the attention of the authors (G. Vachaud, personal communication, 1976) that *Vauclin et al.* [1975] had used permeability values for $\psi < -0.1$ m much lower than those used by *Narasimhan* [1975] and obtained good agreement with experimental observation. A comparison of the permeability characteristics used by *Narasimhan* [1975] and *Vauclin et al.* [1975] is shown in Figure 35.

A subsequent numerical simulation of the same problem based on Vauclin's new physical properties showed that a

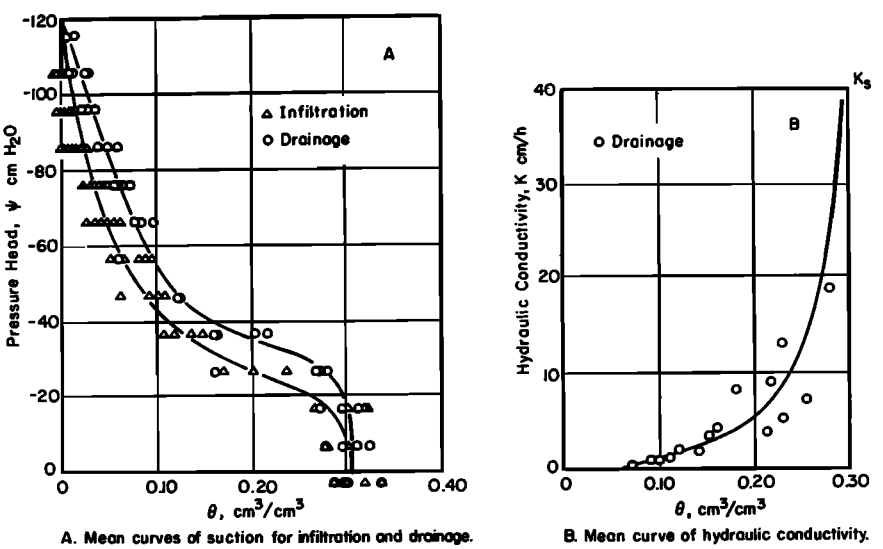

Fig. 30. Drainage from a sandbox: material properties.

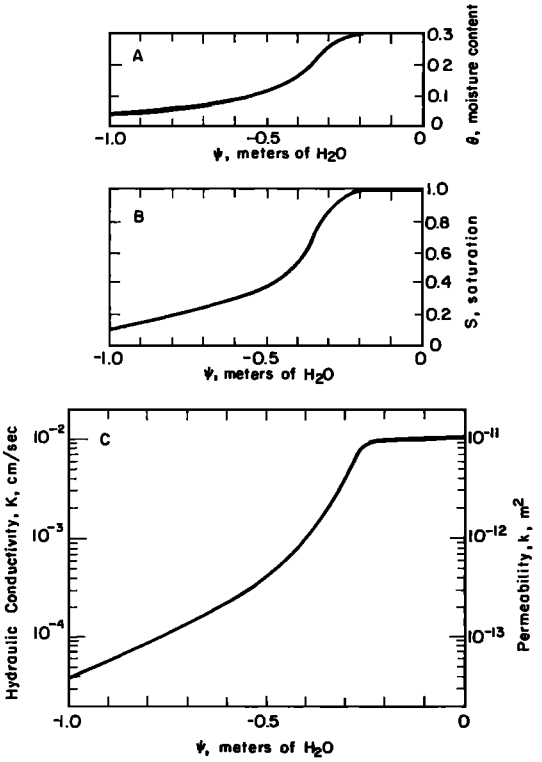

Fig. 31. Drainage from a sandbox: material properties used in the simulation.

much better agreement could be obtained between numerical and experimental values of cumulative depletion from storage (Figure 36).

It may be pointed out here that the use of the new physical properties did not considerably improve the agreement in the position of the surface $\psi = 0$, indicating that the position of the free surface is not very sensitive to changes in physical properties. Moreover, careful study of the simulated results showed that the computation of cumulative storage change was sensitive especially to the permeabilities in the ranges of pressure head less than -0.3 m, confirming the previous inference that the upper left-hand part of the flow region, releasing most of the water from storage and experiencing lowest pressure heads and lowest permeabilities, dominates the unsaturated flow system behavior.

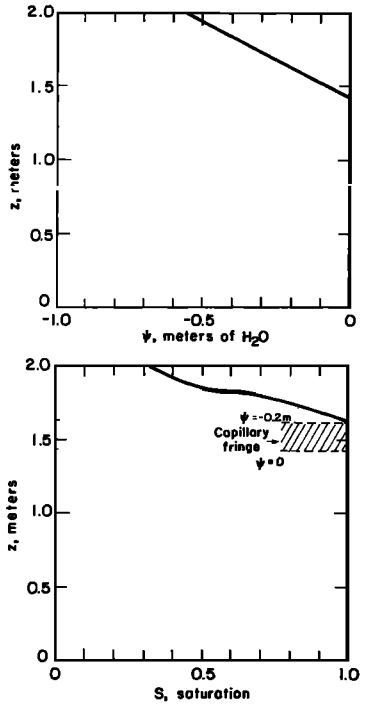

Fig. 32. Drainage from a sandbox: initial distribution of pressure head and moisture content used in the simulation.

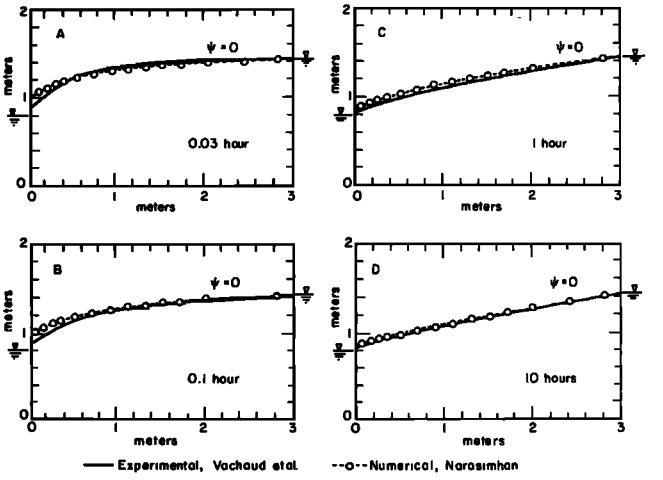

Fig. 33. Drainage from a sandbox: a comparison of numerical and experimental results for the evolution of the surface, $\psi = 0$.

Consolidation Around an Excavation in Soft Clay

Next is a hypothetical problem which is of interest to the soil and foundation engineer and involves settlement associated with the development of moisture suction.

A 20-m bed of soft clay (San Francisco Bay mud), fully saturated up to ground level, is under hydrostatic equilibrium with the fluid potential ϕ, which is everywhere equal to 20 m. The laterally infinite clay bed rests on an impermeable foundation. The upper part of the bed is preconsolidated to 0.35 atm, while the rest is normally consolidated. An excavation 20 m long, 10 m deep, and very wide is made in this bed. The problem is to study the new drainage pattern imposed within the clay bed because of the excavation and the resultant consolidation and swelling phenomena caused by the pore pressure dissipation.

Conceptually, the first step in the solution process is to determine the effect of unloading on the antecedent hydro-

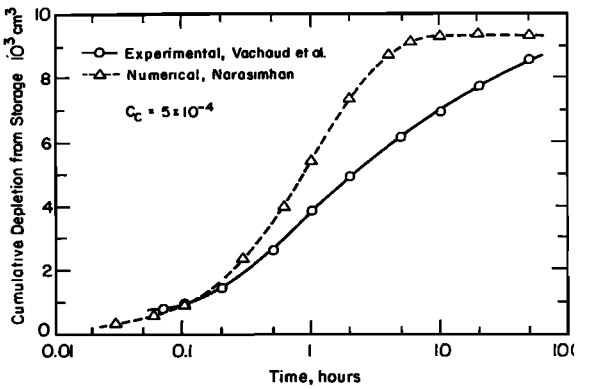

Fig. 34. Drainage from a sandbox: a comparison of numerical and experimental variations of cumulative depletion from storage.

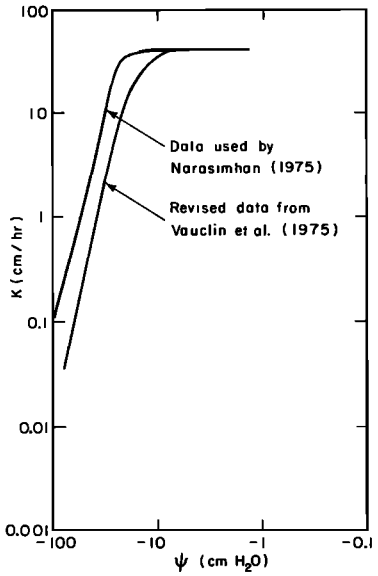

Fig. 35. Drainage from a sandbox: a comparison of permeability characteristics used by *Narasimhan* [1975] and *Vauclin et al.* [1975].

static pore pressure distribution. To do this, it is assumed that (1) the process of excavation is rapid and, considering the low permeability of the clay, can be considered instantaneous and (2) the soil responds elastically in an undrained state in such a way that the change in loading is instantaneously borne by equivalent pore pressure changes and that the soil skeleton does not immediately experience any change in effective stress. With the gradually dissipating pore pressures the effects of unloading are gradually transferred to the soil skeleton.

The initial and boundary conditions of the problem are shown in Figure 37. In order to compute the distribution of ψ and ϕ at $t = 0$ (Figures 37*b* and 37*c*) the following procedure was adopted. Assuming a Poisson's ratio of $\nu = 0.5$, we calculated the new stress distribution at 15 points in the flow region, using the elastic theory stress distribution charts and tables given by *Poulos and Davis* [1974]. The differences between the old and the new stress distribution, evaluated with the help of the Mohr's circle, provided the changes in the principal stresses $\Delta\sigma_1'$, $\Delta\sigma_2'$, and $\Delta\sigma_3'$ ($\Delta\sigma_2' = \Delta\sigma_3'$). The changes in stresses cause changes in pore pressure within the clay. According to *Skempton* [1954], change in pore pressure can be related to effective stresses by the relation

$$\Delta u = \rho_\omega g \Delta\psi = \tfrac{1}{3}(\Delta\sigma_1' + \Delta\sigma_2' + \Delta\sigma_3') \qquad (14)$$

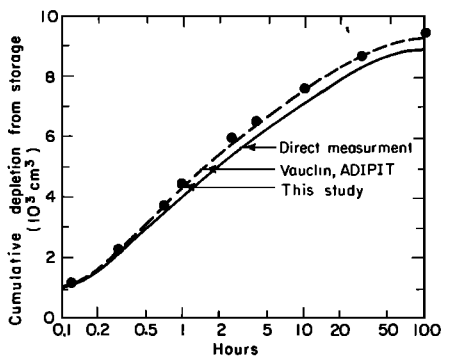

Fig. 36. Drainage from a sandbox: a comparison of experimental and numerical values of cumulative depletion from storage based on *Vauclin et al.*'s [1975] permeability characteristics.

The changes in pore pressure computed by (14) at the 15 control points were contoured to arrive at the new distribution of pore water pressures and potentials, which form the initial conditions for the drainage-settlement problem solved by the numerical model. The initial and boundary conditions of the problem are presented in Figure 37. Note in Figure 37*b* that as a result of the excavation process, a portion of the flow region immediately surrounding the excavation goes into a state of negative pore pressures. We will see later that this has a profound influence on the generation of the seepage face and the settlement in the vicinity of the excavation. In the simulation the floor of the excavation is assumed to be constantly covered by a film of water and hence is treated as a prescribed potential boundary with $\phi = z$. The wall of the excavation is partly impermeable and partly a seepage face, while all the other boundaries are impermeable.

The physical properties of San Francisco Bay mud were experimentally determined by W. N. Houston of the University of California at Berkeley and are presented in Figure 38. These properties represent the 'drained' parameters of the clay. Since the clay is very plastic, it was assumed that desaturation could be initiated only at very large suctions, and that the clay remains fully saturated throughout the range of negative pore pressures encountered in the present problems. The flow region was discretized into 256 volume elements (Figure 39) of unequal size.

The drainage-consolidation computations were carried out for 360 days from $t = 0$, and the distributions of potentials computed at different times are shown in Figure 40.

The evolution of the seepage face in Figure 40 merits special attention. As can be seen from Figure 37*b*, the region immediately around the excavation is in a state of moisture suction at $t = 0$. At $t = 0$ therefore no seepage face could exist along the wall, since by definition water can leave the flow region only across a seepage face. Hence at $t = 0$ the entire wall forms an

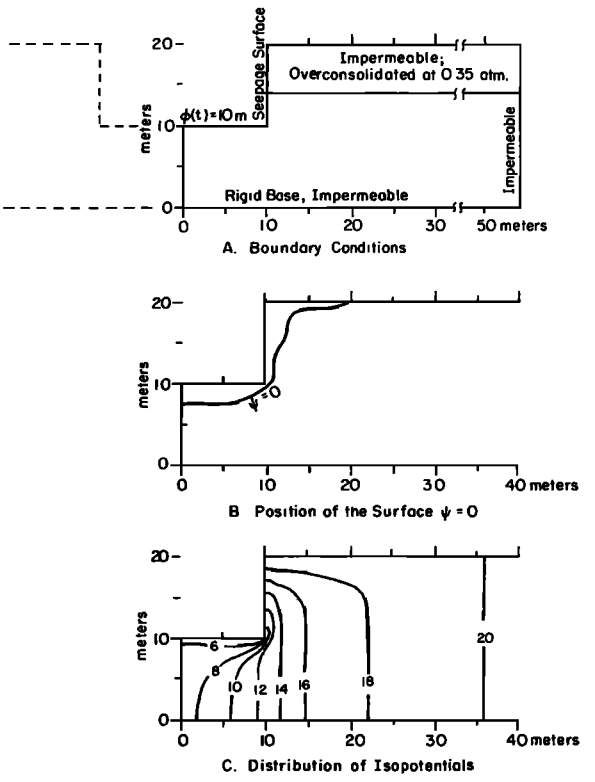

Fig. 37. Excavation in soft clay: initial and boundary conditions.

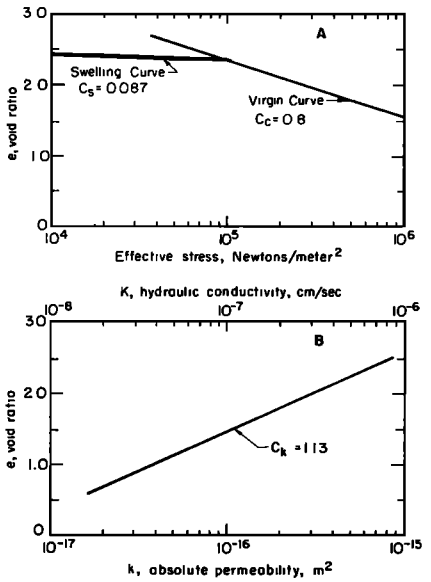

Fig. 38. Excavation in soft clay: physical properties of San Francisco Bay mud (after W. N. Houston, personal communication, 1974).

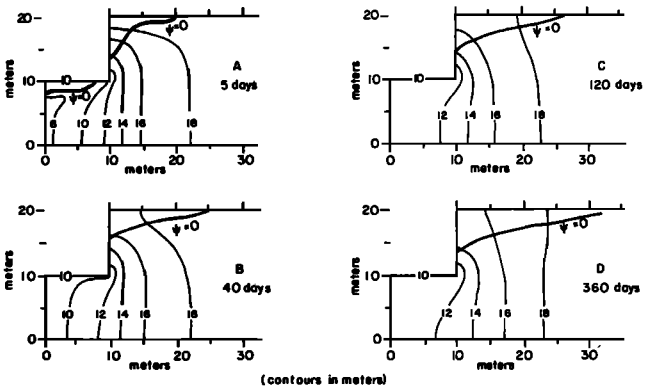

Fig. 40. Excavation in soft clay: isopotentials and the $\psi = 0$ at various times.

impermeable boundary. However, with the passage of time, as pore pressure begins to build up behind the wall, an incipient seepage face forms at the base of the wall and gradually begins to grow upward. As can be seen from Figure 37*b*, the seepage face attains a maximum length after about 40 days and then begins to contract.

The numerical computations provide, for each volume element in the flow region, the total change in volume as a function of time. If we assume that all the volume change takes place in the vertical direction, then the volume change divided by the base area of an element yields the vertical deformation. The summation of the vertical deformations along a given column of volume elements gives the settlement or swelling over the column length.

The pattern of swelling and consolidation around the excavation is illustrated in Figure 41. It can be seen that the floor of the excavation progressively heaves upward with time, the maximum swelling being at the axis of the excavation.

In the region to the right of the excavation the ground gradually settles with time. However, it is interesting to note that the maximum settlement does not occur at the excavation wall but a few meters behind it. The reason for this is as follows: during the initial growth of the seepage face the elements behind the excavation receive more water from the region to the right than can be drained by the still growing seepage face. As a result, these elements experience a net buildup of pore pressure and swell rather than consolidate. As time progresses and the seepage face dominates drainage, these volume elements begin and continue to lose pore pressure and to consolidate.

It would appear that the offset of the trough of maximum consolidation, at some distance behind the excavation wall, is sometimes observed in the field [*Peck*, 1969], as is shown in Figure 42. In this particular case, however, the settlement pattern has been attributed to the inward movement of the vertical wall of the excavation rather than to seepage.

It has been pointed out (R. E. Peck and T. O'Rourke, personal communications, 1977) that in an extremely soft clay, like the one used in the simulation, when elastic theory is used to obtain the initial conditions, the simplified stress calculations may not be completely valid and that therefore other factors should be considered. These assumptions, however, may be valid in less soft materials. It must be emphasized that the purpose of this hypothetical simulation has only been to understand qualitatively the phenomenon of drainage and consolidation around an excavation.

Note that in Figure 41, certain oscillations occur in the settlement profile to the right of the excavation. Whether these are due to the particular initial conditions used or are due to the variation in mesh size is not quite clear.

In a consolidation problem of this nature it is of interest to gain an insight into the pattern of deformation in different parts of the flow domain. The time rates of strain of a few typical points in the flow region are presented in Figure 43.

Figure 43*a* illustrates the behavior of a node which has been undergoing swelling at a progressively decreasing rate with time (by convention, swelling is a negative deformation), while

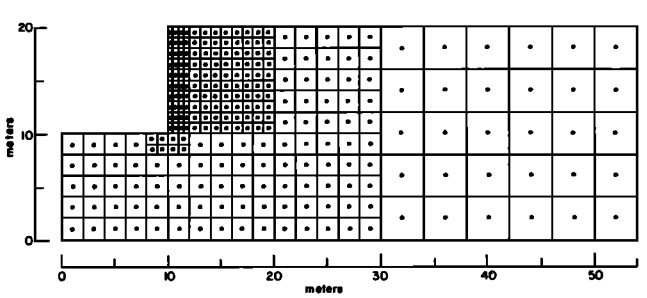

Fig. 39. Excavation in soft clay: discretization of the flow region.

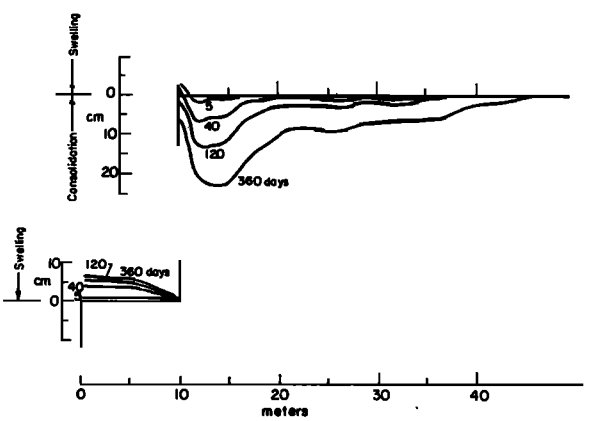

Fig. 41. Excavation in soft clay: pattern of consolidation and swelling.

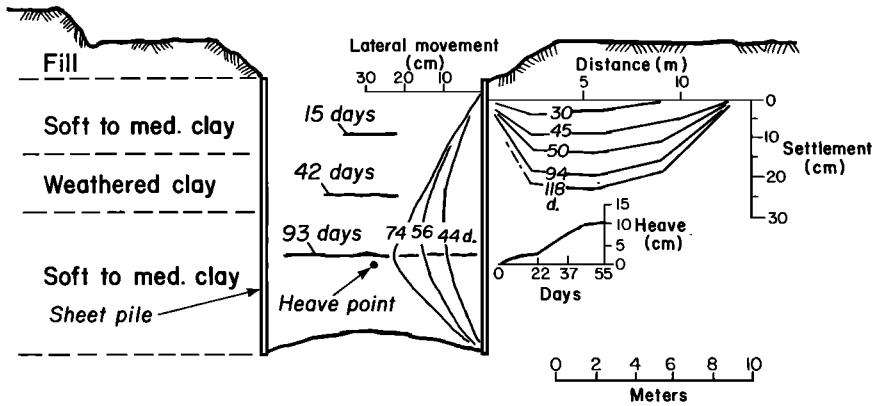

Fig. 42. Relation of the progress of construction to the lateral movement of sheeting and settlements adjacent to an open cut in soft clay in Oslo [after *Peck*, 1969].

Figure 43*b* illustrates an element which has been consolidating ever since $t = 0$. Figure 43*c* summarizes the history of a node which swells slightly to start with, reverses trend, consolidates at an increasing strain rate, attains a peak strain rate, and finally experiences an ever decreasing strain rate. The abrupt increase in strain rate, as evidenced by the inflection in the left limb of the curve in Figure 43*c*, indicates the transition of the node from a state of overconsolidation to one of normal consolidation. Figure 43*d* illustrates the deformation history of a node which passes from an overconsolidated to a normally consolidated state during consolidation. It can be seen that this node attains two peaks of stress rate, one in the domain of recompression and another in the domain of normal consolidation.

Pore Pressure Generation and Dissipation

As the last illustrative example, we will consider the problem of soil liquefaction associated with the response of cohesionless saturated soils to earthquake motion. It is known [*Seed and Lee*, 1966] that cyclic stresses associated with earthquakes and other causes can generate pore pressures in saturated soils. Abnormal buildup of such pore pressures can lead to the loss of strength and consequent liquefaction of shallow cohesionless soils. Liquefaction results when pore pressures equal or exceed existing total stress. In earthquake prone regions, such as coastal California, the design of civil engineering structures must take into consideration the liquefaction potential at the site.

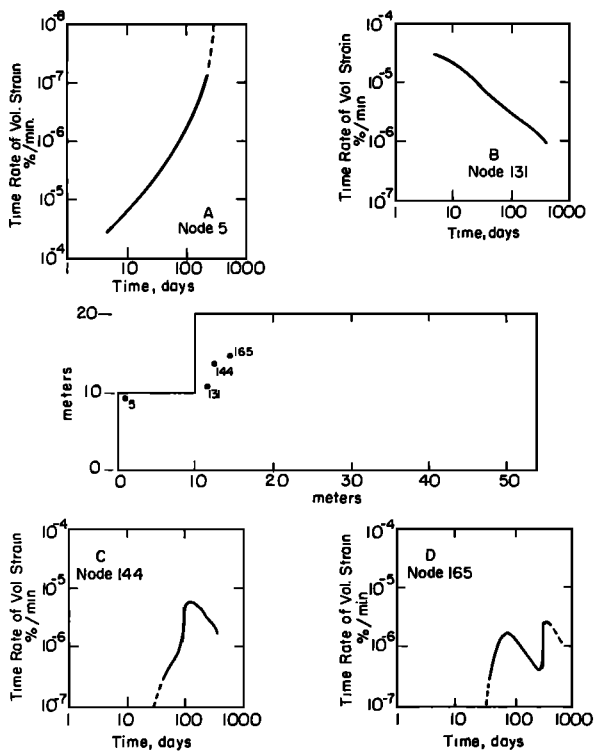

Fig. 43. Excavation in soft clay: time rates of strain of four typical nodes.

On the assumption that liquefaction potential does indeed exist at a given site, one possible method of reducing that potential is the dissipation of pore pressures (concomitant with the generation process) by providing relief drainage wells.

In Figure 44 we consider such a system of drainage wells (with 12-in. diameters) located at 8-ft centers at a site underlain by silty sands intercalated with thin layers of organic material. On considerations of symmetry the shaded region of Figure 44 was modeled as a pie-shaped three-dimensional region, shown in Figure 45.

The system was modeled as a saturated-unsaturated flow region with an initial hydrostatic condition corresponding to the surface $\psi = 0$ located 20 ft below the ground surface. On the basis of design earthquake magnitudes and soil dynamic properties it was calculated by using the method of *Seed et al.* [1975] that the soil would liquefy in a magnitude 7 earthquake lasting for 20 s. In the light of this calculation, appropriate pore pressure generation rates were assigned to each saturated volume element in the flow region. It was assumed from the nature of construction of the relief wells that pore pressure generation would not occur either within the wells or in the unsaturated elements.

The computed results showed that under the given conditions, pore pressures can be dissipated sufficiently during the

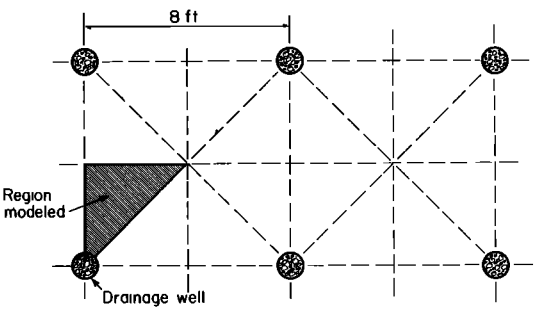

Fig. 44. Liquefaction problem: a plan view of relief drainage wells.

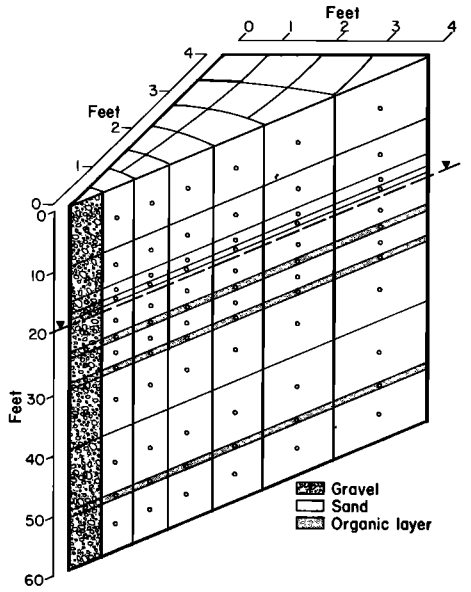

Fig. 45. Liquefaction problem: a three-dimensional model used in simulation.

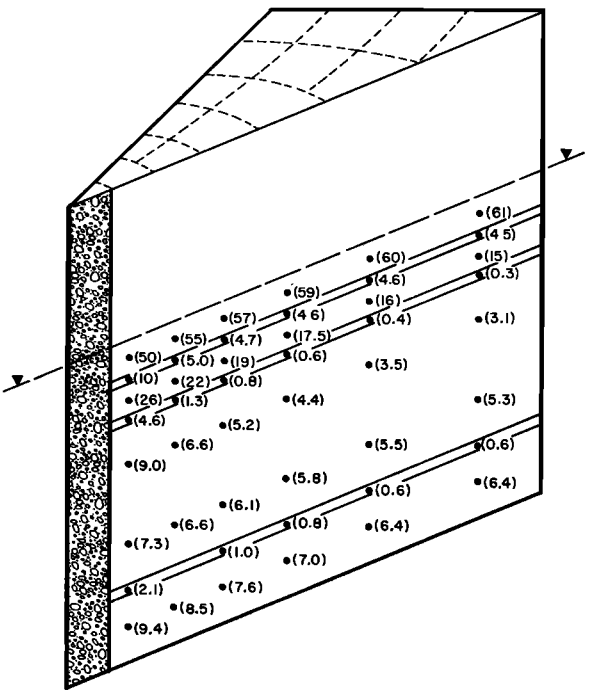

Fig. 46. Liquefaction problem: dissipated pore pressures expressed as a percentage of generated pore pressures at the end of a 20-s magnitude 7 earthquake.

20-s period of the earthquake to minimize the hazard of liquefaction. In particular, the computations showed that the presence of the thin poorly permeable organic layers significantly influences the drainage pattern of the system. Figure 46 presents the pore pressures dissipated during the 20-s period expressed as a percentage of the total pore pressures generated. It is seen that pore pressures are dissipated effectively from within the sands and that difficulty of dissipation is restricted mainly to the organic layers.

NOTATION

a_v coefficient of compressibility, LT^2/M.
C_c compression index, slope of e versus log σ' straight line in the normal consolidation region, 1.
C_k slope of e versus log k straight line, 1.
C_s swelling index, slope of e versus log σ' straight line in the rebound region, 1.
$d_{l,m}$ distance between nodal points l and m, L.
D soil moisture diffusivity, L^2/T.
D_m soil moisture diffusivity in a material coordinate system, L^2/T.
e void ratio, 1.
e_n, e_0 initial and boundary void ratios, respectively, in the clay slurry problem, 1.
g gravitational constant, L/T^2.
k absolute permeability, L^2.
K hydraulic conductivity, L/T.
$K_{l,m}$ mean hydraulic conductivity at interface between nodes l and m, L/T.
K' hydraulic conductivity of aquitard, L/T.
L length of flow column, L.
m material coordinate in the clay slurry problem, L.
m_v volumetric coefficient of compressibility, LT^2/M.
$(M_c)_n$ fluid mass capacity of node n, M/L.
q volumetric flow rate, L^3/T.
r radial distance, L.
S_s coefficient of specific storage, $1/L$.
t time, T.
z elevation, L.
z_l elevation of node l, L.
Γ bounding surface of volume element or flow region, L^2.
$\Gamma_{l,m}$ area of surface element separating volume elements l and m; L^2.
λ Boltzmann's transformation, $L/T^{1/2}$.
θ volumetric moisture content, 1.
μ viscosity, M/LT.
ρ_ω density of water, L^3/T.
σ effective stress, M/LT^2.
σ_1', σ_2', σ_3' principal effective stresses, M/LT^2.
ϕ hydraulic head, L.
χ Bishop's parameter relating ψ and σ' in the unsaturated zone, 1.
ψ pressure head, L.
ψ_l pressure head at nodal point, L.

Acknowledgments. We wish to thank W. N. Houston of the Department of Civil Engineering of the University of California in Berkeley for many stimulating discussions. We also thank John V. Lowney and Associates for permission to include results of the soil liquefaction problem. This work was partly supported by the Division of Geothermal Energy of the U.S. Department of Energy.

REFERENCES

Bruce, R. R., and A. Klute, The measurement of soil-water diffusivity, *Soil Sci. Soc. Amer. Proc., 20,* 458–462, 1956.

De Wiest, R. J. M., Fundamental principles of groundwater flow, in *Flow Through Porous Media,* edited by R. J. M. De Wiest, Academic, New York, 1969.

Hanks, R. J., and S. A. Bowers, Numerical solution of the moisture flow equation for infiltration into layered soils, *Soil Sci. Soc. Amer. Proc., 26,* 530–534, 1962.

Helm, D. C., One-dimensional simulation of aquifer system compaction near Pixley, California, 1, Constant parameters, *Water Resour. Res., 11*(3), 465–478, 1975.

Jacob, C. E., Flow of groundwater, in *Engineering Hydraulics,* edited by Hunter Rouse, John Wiley, New York, 1950.

Liakopoulos, A. C., Transient flow through unsaturated porous media, D. Eng. dissertation, Univ. of Calif., Berkeley, 1965.

Lofgren, B. E., and R. L. Klausing, Land subsidence due to groundwater withdrawal, Tulare-Wasco area, California, *U.S. Geol. Surv. Prof. Pap., 437-B,* 1969.

Narasimhan, T. N., A unified numerical model for saturated-unsaturated groundwater flow, Ph.D. dissertation. Univ. of Calif., Berkeley, 1975.

Narasimhan, T. N., and P. A. Witherspoon, Numerical model for saturated-unsaturated flow in deformable porous media, 1, Theory, *Water Resour. Res., 13*(3), 657–664, 1977.

Narasimhan, T. N., P. A. Witherspoon, and A. L. Edwards, Numerical model for saturated-unsaturated flow in deformable porous media, 2, The algorithm, *Water Resour. Res., 14*(2), 255–261, 1978.

Neuman, S. P., Finite element computer programs for flow in saturated-unsaturated porous media, *Rep. A-10-SWC-77,* Technion Israel Inst. of Technol., Haifa, 1972.

Peck, R. B., Deep excavations and tunneling in soft clay, *Proc. Int. Conf. Soil Mech. Found. Eng. 7th,* 259–265, 1969.

Philip, J. R., Theory of infiltration, *Advan. Hydroscience, 5,* 215–296, 1969.

Poland, J. F., and G. H. Davis, Land subsidence due to withdrawal of fluids, *Rev. Eng. Geol., 2,* 187–269, 1969.

Poulos, H. G., and E. H. Davis, *Elastic Solutions for Soil and Rock Mechanics,* John Wiley, New York, 1974.

Rubin, J., and R. Steinhardt, Soil-water relations during rain infiltration, I, Theory, *Soil Sci. Soc. Amer. Proc., 27,* 246–251, 1963.

Rubin, J., R. Steinhardt, and P. Reiniger, Soil-water relations during rain infiltration, II, Moisture content profiles during rains of low intensities, *Soil Sci. Soc. Amer. Proc., 28,* 1–5, 1964.

Schiffman, R. L., and R. E. Gibson, Consolidation of non-homogeneous clay layers, *J. Soil Mech. Found. Div. Amer. Soc. Civil Eng., 90*(SM5), 1–30, 1964.

Seed, H. B., and K. L. Lee, Liquefaction of saturated sands during cyclic loading, *J. Soil Mech. Found. Div. Amer. Soc. Civil Eng. 92*(SM6), 105–134, 1966.

Seed, H. B., P. P. Martin, and J. Lysmer, The generation and dissipation of pore water pressures during soil liquefaction, *Rep. EERC 75-26,* Earthquake Eng. Res. Center, Univ. of Calif., Berkeley, 1975.

Skempton, A. W., The pore pressure coefficients *A* and *B, Geotechnique, 4,* 143–147, 1954.

Smiles, D. E., Infiltration into a swelling material, *Soil Sci., 117*(3), 140–147, 1974.

Smiles, D. E., and M. J. Rosenthal, The movement of water in swelling materials, *Aust. J. Soil. Res., 6,* 237–248, 1968.

Terzaghi, K., Principles of soil mechanics, a summary of experimental results of clay and sand, *Eng. News Rec., 269,* 3–98, 1925.

Vachaud, G., M. Vauclin, J. L. Thony, and D. Khanji, Etude expérimentale du drainage de la recharge des nappes à surface libre dans un modele bidimensionel, report, Lab. des Mec. des Fluides, Univ. Sci. et Med. de Grenoble, Grenoble-Crane, France, 1971.

Vauclin, M., G. Vachaud, and D. Khanji, Two dimensional numerical analysis of transient water transfer in saturated-unsaturated soils, in *Computer Simulations in Water Resources Systems,* edited by G. C. Vansteenkiste, North-Holland, Amsterdam, 1975.

(Received June 8, 1978;
accepted June 20, 1978.)